

Quantum Sensing of Geomagnetic Fluctuations and Noise Spectroscopy With Hybrid Short Ramsey-Haar Wavelet Method and NV Ensembles

CHOU-WEI KIANG¹ and JEAN-FU KIANG^{1 2}, (LIFE SENIOR, IEEE)

¹Department of Electrical Engineering, National Taiwan University, Taipei, Taiwan 10617

²Graduate Institute of Communication Engineering, National Taiwan University, Taipei, Taiwan 10617

Corresponding author: Jean-Fu Kiang (email: jfkiang@ntu.edu.tw).

ABSTRACT

A robust quantum sensing method based on nitrogen-vacancy (NV) ensembles is proposed to reconstruct the geomagnetic fluctuations in the VLF (3-30 kHz) band, which is known to correlate with seismic and solar activities. Short Ramsey sequences and Haar wavelet method are proposed to reconstruct the dc and ac components, respectively, of an arbitrary time-domain waveform. A sensitivity of $0.63 \text{ pT}/\sqrt{\text{Hz}}$ can be achieved by using multiple NV ensembles (NVEs), with each containing $N = 10^8$ uncorrelated NV centers. Our simulation results indicate that the signal-to-noise ratio (SNR) and sensitivity are proportional to $N^{0.4}$, which is below the standard quantum limit due to pure dephasing. The spin-bath noise spectroscopy can also be achieved by observing the fluorescence emission from batches of NV centers in an NVE. The parameters characterizing the noise spectrum are estimated by using a particle swarm optimization (PSO) algorithm. The efficacy of the proposed method is validated by reconstructing a geomagnetic waveform recorded in the DEMETER satellite mission. NVE-based quantum sensors operated with the proposed hybrid short Ramsey-Haar wavelet method can be installed on nano-satellites to monitor the global geomagnetic fluctuations with fine temporal resolution of μs and superior sensitivity of $\text{sub-pT}/\sqrt{\text{Hz}}$.

INDEX TERMS Quantum sensing, nitrogen-vacancy (NV) ensemble, waveform reconstruction, geomagnetic field, spin-bath noise, Ramsey sequence, spin-echo sequence, Haar wavelet

I. INTRODUCTION

NEGATIVELY charged nitrogen-vacancy (NV) centers in diamond have been engineered for high-resolution and high-sensitivity sensing of magnetic and electric fields, mechanical strain and temperature [1]. Ensemble of NV centers can be used for wide-field microscopic imaging, facilitating in-situ studies of electronic, chemical and biological devices [2], [3]. Recently, NV centers were explored for novel applications in navigation [4], biological electromagnetism at cellular level [5], and condensed matter physics like probing superconducting vortices and noise currents [6].

Besides their versatile applications, NV centers can tolerate harsh environments with temperature from cryogenic to 600 K and high pressure over 13 GPa [5]. These merits make NV centers and NV ensembles (NVEs) viable as satellite-borne sensors for space explorations. However, satellite-borne quantum sensors for geomagnetic detection

were rarely discussed. In [7], low-frequency geomagnetic-field intensity was detected by using a hybrid technique based on NV-optically detected magnetic resonance (ODMR) and magnetic flux concentrator. The idea of using quantum sensors for detecting geomagnetic fluctuations at kHz frequency and sub-nT level was not found in the literature.

The geomagnetic field intensity in the ionosphere is about tens of thousands nT [8], mainly induced by current sources in the Earth's core. Seismic activities and external sources, such as solar activities, give rise to much weaker geomagnetic fluctuations in the ionosphere and the magnetosphere [9], [10]. These fluctuations are in sub-nT level during geomagnetically quiet period, but may reach thousands of nT in severely disturbed events [8].

Global monitoring of geomagnetic field can provide valuable information for geophysics studies on the Earth's crust. The temporal and spatial distributions of geomagnetic fluc-

tuations are valuable for researches on seismology [11] and geomagnetic interaction with solar activities.

The DEMETER is a micro-satellite mission launched by CNES for seismo-electromagnetic studies and was concluded in Dec. 2010 [12]. Electromagnetic signals recorded by the DEMETER satellites have been used to study the ionospheric response to anthropogenic activities and natural phenomena like earthquakes, tsunamis and volcanic activities [11]. The DEMETER mission provided waveforms and spectra of magnetic field in ELF (3 Hz-3 kHz) and VLF (3 kHz-30 kHz) bands [13], which were used to explore seismo-magnetic phenomena [14], [15] and geomagnetic storms induced by solar wind [16], [17].

The Swarm low-earth-orbit (LEO) satellite constellation was deployed by the European Space Agency (ESA) and is currently operational at altitude of 450 km for observing the Earth's magnetic field [18]. The onboard vector field magnetometer (VFM) has a wide dynamic range from sub-nT to over 65,000 nT, at the sensitivity of a few nT/ $\sqrt{\text{Hz}}$ [18]. However, its sampling rate is only 50 Hz and its operating temperature is limited between -20 and 40°C [18].

NVE-based magnetometers can provide higher sensitivity, finer resolution, and stronger environmental resilience than the existing VFMs. A quantum sensing network [19], [20] can be formed by installing NVE-based quantum sensors on nano-satellites to observe geomagnetic field with global coverage, achieving time resolution of microseconds and sensitivity of pT/ $\sqrt{\text{Hz}}$ in the kHz band [21].

Since the readout signals from individual NV centers are uncorrelated, the sensitivity and the signal-to-noise ratio (SNR) of an NVE-based magnetometer can be improved by a factor of \sqrt{N} if N NV centers are fabricated in an NVE or N individual readouts are performed [22], [21]. For example, an NVE containing $\sim 10^{11}$ NV centers in a volume of $8.5 \times 10^{-4} \text{ mm}^3$ was reported for quantum sensing at room temperature [21]. The sensitivity of NV centers is proportional to $1/\sqrt{T_s}$, where T_s is the sensing time. With $T_s = 100$ s, the sensitivity can reach $0.9 \text{ pT}/\sqrt{\text{Hz}}$ at 20 kHz, and can be further improved to fT/ $\sqrt{\text{Hz}}$ by applying dynamical decoupling (DD) technique [21].

Despite numerous merits offered by high-sensitivity NVE-based magnetometers, inevitable challenges of decoherence and dephasing need to be overcome. Magnetometers with sensitivity better than $10 \text{ pT}/\sqrt{\text{Hz}}$ are vulnerable to the environmental noise [23]. The spin relaxation time T_1 of NV center exceeds 6 ms at room temperature, and the spin dephasing time T_2 can be extended to T_1 by applying DD techniques [23] to suppress pure dephasing and attenuate the qubit-environment interaction [1], [24]. DD sequences have been used to reconstruct the spectrum of surrounding noise [25], [26], which can be used to customize MW pulses for reducing qubit error rate [25].

The DD technique is the extension of a spin-echo (SE) sequence, in which a π -pulse is inserted in the middle of the total sensing period to reinstate the sensitivity of detecting an ac signal [1]. The filter function of an SE sequence

has similar features of a Haar wavelet function. A Haar coefficient can be determined from the readout of an NV center after applying a proper SE sequence [27]. In [27], a Haar wavelet method was proposed for detecting nerve impulses, and a proof-of-concept experiment was conducted on rescaled signals of few hundreds nT in magnitude. However, the method in [27] is only applicable to signals that fluctuate around zero, and the decoherence and dephasing issues were not elaborated. Inspired by this study, we extend the Haar wavelet method to perform noise spectroscopy and sense the geomagnetic fluctuations with typical magnitude below 0.1 nT in the VLF band of 3-30 kHz.

In this work, we propose a hybrid short Ramsey-Haar wavelet method to operate a set of NVE-based quantum sensors for the reconstruction of a weak and arbitrary waveform with non-zero mean, as well as the spin-bath noise spectrum. The waveform is represented in terms of Haar wavelet functions, with Haar coefficients and dc coefficient determined by applying SE sequences and short Ramsey sequences, respectively. In the meantime, the spin-bath noise spectrum can be acquired by applying the proposed method to read out a small portion of NV centers in each NVE. Simulations are conducted to reconstruct a geomagnetic waveform extracted from the DEMETER database in the VLF band. The sensitivity and accuracy of the proposed concept are also analyzed by simulations.

The rest of this work is organized as follows. The concept and the simulation scenario are elaborated in Section II. Theories of waveform reconstruction and the relation between noise waveform and Lorentzian spin-bath noise spectrum are presented in Section III. Then, the waveform of geomagnetic fluctuations and the spin-bath noise spectrum, respectively, are reconstructed by simulations and analyzed in Section IV. Finally, some conclusions are drawn in Section V.

II. CONCEPT AND SIMULATION SCENARIO

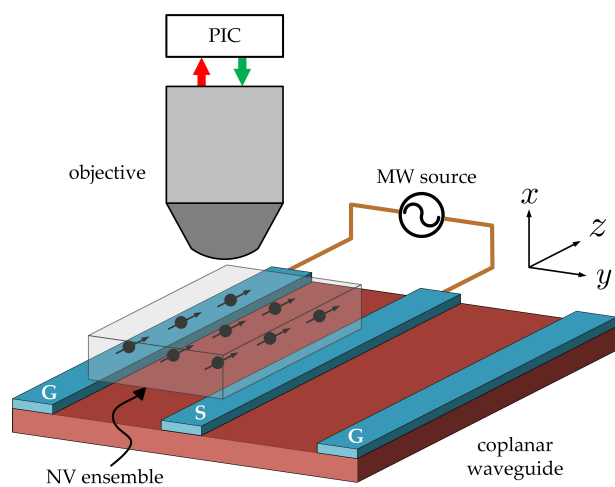


FIGURE 1. Concept of reconstructing geomagnetic fluctuations and spin-bath noise spectrum with NV ensembles (NVEs), where photonic integrated circuit (PIC) is used to initialize the NV ensemble and readout fluorescence signal.

Fig.1 shows the concept of reconstructing the geomagnetic fluctuations and spin-bath noise spectrum with NV ensembles (NVEs). Each NVE is independently controlled with a short Ramsey sequence or an SE sequence guided along a coplanar waveguide (CPW) [28]. The output fluorescence from the NVE can be collected with a photodiode [28] and mapped to a specific dc offset coefficient or Haar coefficient for reconstructing the waveform of geomagnetic fluctuations.

To reconstruct the noise spectrum, fluorescence information from batches of NV centers in an ensemble is retrieved by using a CCD camera chip with supporting photonic integrated circuit (PIC) [21], [29]. This NVE should have sufficiently low concentration such that NV centers in small batch size can be spatially resolved and readout.

A. SAMPLES OF NV ENSEMBLE

In [30], the properties of three NV-center samples in diamond at room temperature were analyzed. For quantum sensing applications, NVEs with longer spin coherence time is desirable to attain better sensitivity, which can be achieved by applying proper DD sequence or preparing an isotopically pure ^{12}C sample [31]. Each NVE sample considered in our simulations is isotopically enriched in ^{12}C , with NV concentration of $10^{14}/\text{cm}^3$ [30] and volume of 10^{-3} mm^3 , containing 10^8 NV centers. The spin-echo coherence time of an ^{12}C NVE sample with nitrogen concentration of 1 ppm is $T_2 = 270\mu\text{s}$ [30]. Since the Ramsey coherence time T_2^* was not available, we assume $T_2^* \simeq 70\mu\text{s}$.

Table 2 lists the default parameters used in the simulations. A static magnetic field of $B_s = 50 \text{ G}$ is applied to distinguish the transitions $|m_s = 0\rangle \leftrightarrow |m_s = +1\rangle$ and $|m_s = 0\rangle \leftrightarrow |m_s = -1\rangle$ in the ground triplet state of an NV center. The transition $|m_s = 0\rangle \leftrightarrow |m_s = -1\rangle$ is chosen as the qubit (two-level system) in our simulations. We will refer to this two-level system based on single NV center as the NV qubit in this work.

B. GENERATION OF SPIN-BATH NOISE

The coupling between NV spins and nitrogen spin-bath is characterized with a Lorentzian noise spectrum [30]

$$S(\omega) = \frac{\Delta^2 \tau_c}{\pi} \frac{1}{1 + (\omega \tau_c)^2} \quad (1)$$

where $\Delta = 30 \text{ kHz}$ is the coupling strength, and $\tau_c = 10\mu\text{s}$ is the correlation time of the spin-bath in a ^{12}C sample. With low ^{13}C nuclear spin impurity and low nitrogen concentration, the ^{12}C sample has the smallest coupling strength between the NV-spin and the nitrogen spin-bath among the three samples discussed in [30].

In the simulations, the time series of Gaussian noise colored by the Lorentzian noise spectrum in (1) is generated by using a Python PyCBC toolbox [32]. An independent noise time series is simulated for each of the 10^8 NV centers contained in an NV ensemble.

C. WAVEFORM OF GEOMAGNETIC FLUCTUATIONS

Fig.2 shows the waveform of geomagnetic fluctuations used in our simulations, which is extracted from the CNES-CDPP database [13] in the VLF band, recorded by the DEMETER satellite, dated 10:51:41.149 UTC on July 1, 2008. The waveform was recorded at sampling rate of 40 kHz [12], which is interpolated to time steps of $0.5\mu\text{s}$ for simulating the spin evolution. The waveform is segmented into 10 uniform intervals of $256 \mu\text{s}$, to ensure that the sensing time T_s in each interval is less than T_2 and that of the short Ramsey sensing time T'_s is less than T_2^* . The reconstructed waveform from all the intervals are concatenated to obtain a whole waveform of geomagnetic fluctuations.

TABLE 1. Default parameters used in simulations.

parameter	symbol	value	ref.
zero-field splitting	$D_{gs}/(2\pi)$	2.87 GHz	[21]
electron spin gyromagnetic ratio	$\gamma_e/(2\pi)$	2.802 MHz/G	[21]
spin-bath coupling strength	Δ	30 kHz	[30]
spin-bath correlation time	τ_c	$10 \mu\text{s}$	[30]
bias magnetic field	B_s	50 G	[30]
NVE density	n_{NV}	10^{14} cm^{-3}	[30]
NV centers per NVE	N	10^8	
Ramsey coherence time	T_2^*	$70 \mu\text{s}$	
spin-echo coherence time	T_2	$270 \mu\text{s}$	[30]
sensing time per interval	T_s	$256 \mu\text{s}$	
short Ramsey sensing time	T'_s	$64 \mu\text{s}$	
Haar-wavelet order	M	8	

III. THEORIES OF WAVEFORM RECONSTRUCTION

Fig.2 demonstrates the concept of waveform reconstruction with the hybrid short Ramsey-Haar wavelet method. Four consecutive short Ramsey sequences (R_ℓ with $\ell = 1, 2, 3, 4$) are applied to measure the residual dc offset in four different NVEs, and SE sequences are applied to designate NVEs to determine the Haar wavelet coefficients up to the M th-order (H_m^n , with $m = 0, \dots, M-1$ and $n = 0, 1, \dots, 2^m - 1$). In this work, a total of $N_e = 4 + (2^0 + 2^1 + \dots + 2^7) = 259$ NVEs are deployed to reconstruct a geomagnetic waveform up to the eighth-order along the direction of NV axes. The response of individual NV qubits in an NVE are statistically superposed to form the fluorescence response of the NVE.

A. SPIN-ECHO SEQUENCES IN HAAR WAVELET METHOD

The Haar mother wavelet function is defined as [33]

$$\psi(x) = \begin{cases} 1, & 0 \leq x < 1/2 \\ -1, & 1/2 \leq x < 1 \\ 0, & otherwise \end{cases} \quad (2)$$

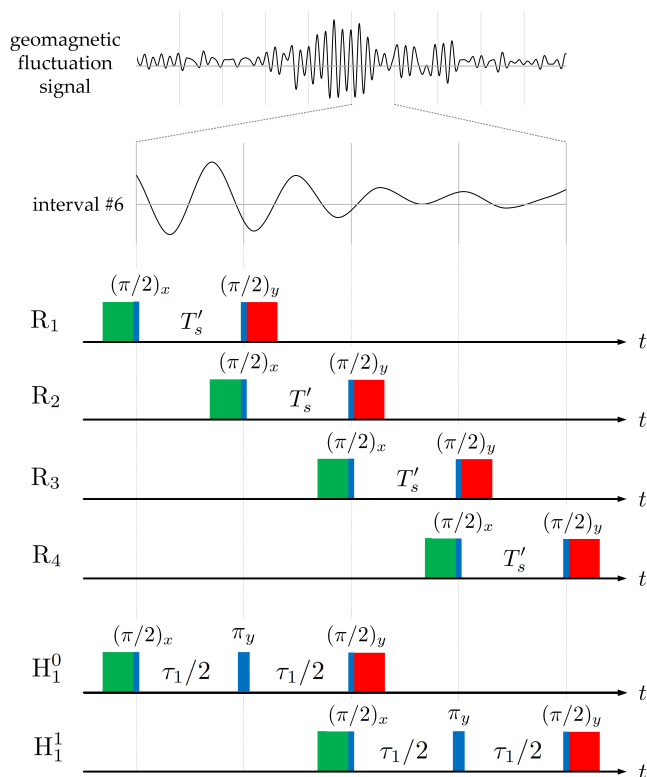


FIGURE 2. Reconstruction of arbitrary waveform with short Ramsey sequences (R_ℓ with $\ell = 1, 2, 3, 4$) and spin-echo sequences for implementing Haar wavelet method (H_m^n with $m = 0, \dots, M-1$ and $n = 0, 1, \dots, 2^m - 1$; SE sequences of $m = 1$ are demonstrated). Microwave (MW) control pulses are marked blue. Optical excitation pulses for initialization and readout are marked green and red, respectively.

which is dilated and translated to form a complete and orthonormal basis $\{h_m^n(x)\}$. The n th Haar function of order m is given by [33], [34]

$$h_m^n(x) = \sqrt{2^m} \psi(2^m x - n) \\ = \begin{cases} 2^{m/2}, & \frac{n}{2^m} \leq x < \frac{n+1/2}{2^m} \\ -2^{m/2}, & \frac{n+1/2}{2^m} \leq x < \frac{n+1}{2^m} \\ 0, & \text{otherwise} \end{cases} \quad (3)$$

where $m = 0, 1, \dots, M-1$ and $n = 0, 1, \dots, 2^m - 1$.

An arbitrary signal $f(x)$ with finite energy defined over $x \in [0, 1]$ can be represented in terms of the Haar wavelet bases as [33]

$$f(x) = d + \sum_{m=0}^{\infty} \sum_{n=0}^{2^m-1} c_{mn} h_m^n(x) \quad (4)$$

where d is the dc offset, and

$$c_{mn} = \langle f, h_m^n \rangle = \int_0^1 f(x) h_m^n(x) dx \quad (5)$$

is the Haar coefficient of $h_m^n(x)$, which is related to the accumulated phase ϕ_{mn} of a spin-echo sequence flipped in time according to the pattern of $h_m^n(x)$.

Given the sensing time per interval, T_s , the inter-pulse spacing of h_m^n is $\tau_m = T_s/2^m$. The phase retrieved from the geomagnetic waveform $B(t)$ with the modulation function $h_m^n(t)$ is given by

$$\phi_{mn} = \int_{nT_s/2^m}^{(n+1/2)T_s/2^m} \gamma_e B(t) dt \\ - \int_{(n+1/2)T_s/2^m}^{(n+1)T_s/2^m} \gamma_e B(t) dt = c_{mn} \gamma_e \tau_m 2^{m/2} \quad (6)$$

leading to

$$c_{mn} = \frac{2^{-m/2}}{\gamma_e \tau_m} \phi_{mn} \quad (7)$$

If the geomagnetic field $B_f(t)$ is polarized along the NV axis (z -axis), and the magnetic field of the spin-bath noise is $b_z(t)$, then the Hamiltonian of the NV qubit in the lab frame is given by

$$H(t) = \frac{1}{2} \hbar \omega_0 \sigma_z + \frac{1}{2} \hbar \gamma_e B_z(t) \sigma_z \quad (8)$$

where

$$B_z(t) = B_f(t) + b_z(t) \quad (9)$$

is the effective time-dependent magnetic field sensed by the NV qubit,

$$\omega_0 = D_{gs} - \omega_s = D_{gs} - \gamma_e B_s \quad (10)$$

is the Larmor frequency under the bias field B_s , and D_{gs} is the zero-field splitting of the NV center.

The Hamiltonian of the NV qubit in the rotating frame with Larmor frequency ω_0 is given by

$$H_r(t) = U_r^\dagger H U_r - i \hbar U_r^\dagger \dot{U}_r = \hbar \gamma_e B(t) \sigma_z \quad (11)$$

where $U_r = e^{-i\omega_0 t \sigma_z/2}$ is the transformation operator and $U_r^\dagger \sigma_z U_r = \sigma_z$. The NV qubit evolves in the rotating frame according to the operator

$$U_e(t_0, t) = \exp \left\{ -\frac{i}{\hbar} \int_{t_0}^t H_r(t') dt' \right\} \quad (12)$$

The phase ϕ_{mn} is retrieved by exerting a spin-echo sequence H_m^n as illustrated in Fig. 2. A $(\pi/2)_x$ -pulse is applied to drive the initial state $|0\rangle$ of the NV qubit to the state

$$|\psi_0\rangle = \frac{1}{\sqrt{2}}(|0\rangle - i|1\rangle) \quad (13)$$

Then, the NV qubit is driven by the SE sequence H_m^n as follows.

- 1) The NV qubit evolves freely under operator $U_e \left(\frac{nT_s}{2^m}, \frac{(n+1/2)T_s}{2^m} \right)$.
- 2) Apply an instant π_y -pulse.
- 3) The NV qubit evolves freely under operator $U_e \left(\frac{(n+1/2)T_s}{2^m}, \frac{(n+1)T_s}{2^m} \right)$.

- 4) Apply an instant $(\pi/2)_y$ -pulse, then readout the fluorescence.

After step 1, the state of NV qubit becomes

$$|\psi_1\rangle = \frac{1}{\sqrt{2}}e^{-i\phi_1/2}(|0\rangle - ie^{i\phi_1}|1\rangle) \quad (14)$$

where

$$\phi_1 = \gamma_e \int_{nT_s/2^m}^{(n+1/2)T_s/2^m} B(t)dt \quad (15)$$

After a π_y -pulse is exerted on $|\psi_1\rangle$ in step 2 and the time evolution in step 3, we have

$$|\psi_3\rangle = \frac{1}{\sqrt{2}}ie^{i\phi_{mn}/2}(|0\rangle - ie^{-i\phi_{mn}}|1\rangle) \quad (16)$$

where

$$\begin{aligned} \phi_{mn} = \gamma_e & \left[\int_{nT_s/2^m}^{(n+1/2)T_s/2^m} B(t)dt \right. \\ & \left. - \int_{(n+1/2)T_s/2^m}^{(n+1)T_s/2^m} B(t)dt \right] \end{aligned} \quad (17)$$

After exerting a $(\pi/2)_y$ -pulse on $|\psi_3\rangle$, we obtain

$$|\psi_f\rangle = \frac{1}{2}ie^{i\phi_{mn}/2} \begin{bmatrix} 1 + ie^{-i\phi_{mn}} \\ 1 - ie^{-i\phi_{mn}} \end{bmatrix} \quad (18)$$

Then, the probability of the system being at $|0\rangle$ is

$$P_{m,0 \rightarrow 0}^n = |\langle 0 | \psi_f \rangle|^2 = \frac{1}{2}(1 + \sin \phi_{mn}) \quad (19)$$

Finally, the accumulated phase is estimated as

$$\phi_{mn} = \sin^{-1}(2P_{m,0 \rightarrow 0}^n - 1) \quad (20)$$

B. SHORT RAMSEY SEQUENCES FOR SENSING DC OFFSET

While Haar wavelet functions are used to extract high-frequency components, the quasi-dc components in the waveform can be captured by using the associated scaling function [34]

$$\phi_s(x) = \begin{cases} 1, & 0 \leq x < 1 \\ 0, & \text{otherwise} \end{cases} \quad (21)$$

The scaling function resembles the time-domain filter function of a Ramsey sequence. However, if the dc offset is significant, the accumulated phase in the NV qubit retrieved with a conventional Ramsey sequence over T_s may exceed 2π , leading to phase ambiguity. In this work, N_R short Ramsey sequences with sensing time of $T'_s = T_s/N_R$ are consecutively applied to retrieve the phases in an NVE for estimating the dc offset.

Referring to Fig.2, the phase accumulated in the NV qubit, induced by a short Ramsey sequence R_ℓ , is retrieved as follows.

- 1) Apply an instant $(\pi/2)_x$ -pulse on the NV qubit after initialization.
- 2) The NV qubit evolves freely under operator $U_e((\ell - 1)T'_s, \ell T'_s)$.
- 3) Apply an instant $(\pi/2)_y$ -pulse on the NV qubit before readout the fluorescence.

After the NV qubit is initialized at state $|0\rangle$, its state after steps 1 and 2 becomes

$$|\psi_1\rangle = \frac{1}{\sqrt{2}}e^{-i\varphi_\ell/2}(|0\rangle - ie^{i\varphi_\ell}|1\rangle) \quad (22)$$

where

$$\varphi_\ell = \gamma_e \int_{(\ell-1)T'_s}^{\ell T'_s} B(t)dt = \gamma_e T'_s d_\ell \quad (23)$$

After step 3, the phase becomes

$$|\psi_f\rangle = \frac{1}{2}e^{-i\varphi_\ell/2} \begin{bmatrix} 1 + ie^{i\varphi_\ell} \\ 1 - ie^{i\varphi_\ell} \end{bmatrix} \quad (24)$$

The probability of the NV qubit being at $|0\rangle$ is computed as

$$P_{\ell,0 \rightarrow 0} = |\langle 0 | \psi_f \rangle|^2 = \frac{1}{2}(1 - \sin \varphi_\ell) \quad (25)$$

Hence, the accumulated phase is determined as

$$\varphi_\ell = \sin^{-1}(1 - 2P_{\ell,0 \rightarrow 0}) \quad (26)$$

Finally, the dc offset coefficient over $0 \leq t \leq T_s$ is estimated as

$$d = \frac{1}{\gamma_e N_R T'_s} \sum_{\ell=1}^{N_R} \varphi_\ell \quad (27)$$

C. RECONSTRUCTION OF GEOMAGNETIC WAVEFORM

Theoretically, a single NV qubit can be used to reconstruct the geomagnetic waveform in the absence of noise. However, it is very challenging to excite and readout a single NV qubit in a practical diamond sample, especially when the spin-bath noise is much stronger than the weak geomagnetic fluctuations. There are N_e NVEs in the simulation scenario, with each containing N NV centers, and thus N NV qubits. We assume that all these NV qubits sense the same geomagnetic fluctuations, but different spin-bath noise. By using the concept shown in Fig.1 to reconstruct the geomagnetic fluctuations, we first estimate the ensemble average of the transition probabilities in each NVE as

$$\bar{P}_{m,0 \rightarrow 0}^n = \frac{1}{N} \sum_{p=1}^N P_{mp,0 \rightarrow 0}^n \quad (28)$$

$$\bar{P}_{\ell,0 \rightarrow 0} = \frac{1}{N} \sum_{p=1}^N P_{\ell p,0 \rightarrow 0} \quad (29)$$

where $P_{mp,0 \rightarrow 0}^n$ and $P_{\ell p,0 \rightarrow 0}$ for the p th NV qubit in an NVE are defined in (19) and (25), respectively. The noise effects are mitigated by taking the ensemble average, revealing the information pertinent to geomagnetic fluctuations.

Then, the Haar coefficients and the dc offset coefficient contributed by the geomagnetic fluctuations are estimated as

$$\bar{c}_{mn} = \frac{2^{-m/2}}{\gamma_e \tau_m} \bar{\phi}_{mn} = \frac{2^{-m/2}}{\gamma_e \tau_m} \sin^{-1}(2\bar{P}_{m,0 \rightarrow 0}^n - 1) \quad (30)$$

$$\bar{d} = \frac{1}{\gamma_e N_R T'_s} \sum_{\ell=1}^{N_R} \bar{\varphi}_\ell = \frac{1}{\gamma_e N_R T'_s} \sum_{\ell=1}^{N_R} \sin^{-1}(1 - 2\bar{P}_{\ell,0 \rightarrow 0}) \quad (31)$$

Finally, the geomagnetic waveform is reconstructed as

$$\tilde{B}(t) = \bar{d} + \sum_{m=0}^M \sum_{n=0}^{2^m-1} \bar{c}_{mn} h_m^n(t) \quad (32)$$

D. EFFECTS OF TRANSVERSE MAGNETIC FIELD

Previously, we focused on the scenario with magnetic field polarized along the z -direction. However, the geomagnetic field is not generally polarized in the z direction. If a transverse magnetic field of x polarity is exerted on the NV qubit, the Hamiltonian in the lab frame is given by

$$H_x(t) = \frac{1}{2}\hbar\omega_0\sigma_z + \frac{1}{2}\hbar\gamma_e B_x(t)\sigma_x \quad (33)$$

and that in the rotating frame with Larmor frequency ω_0 is

$$H_{rx}(t) = \frac{1}{2}\hbar\gamma_e B_x(t)[\cos(\omega_0 t)\sigma_x - \sin(\omega_0 t)\sigma_y] \quad (34)$$

with

$$U_r^\dagger \sigma_x U_r = \cos(\omega_0 t)\sigma_x - \sin(\omega_0 t)\sigma_y \quad (35)$$

Before applying a spin-echo sequence H_m^n or a short Ramsey sequence R_ℓ , the NV qubit is initialized to state $|0\rangle$, followed by a $(\pi/2)_x$ -pulse to reach the state

$$|\psi_0\rangle = \frac{1}{\sqrt{2}} \begin{bmatrix} 1 & -i \\ -i & 1 \end{bmatrix} \begin{bmatrix} 1 \\ 0 \end{bmatrix} = \frac{1}{\sqrt{2}}(|0\rangle - i|1\rangle) \quad (36)$$

Then, the NV qubit evolves according to an operator $U_e(0, T_s/2) \simeq \bar{I}$ if $B_x(t)$ is on the order of 10^{-6} T during $[0, T_s]$ and ω_0 is on the order of GHz, reaching the state

$$|\psi_1\rangle \simeq |\psi_0\rangle \quad (37)$$

After applying a π_y -pulse on $|\psi_1\rangle$, we have

$$|\psi_2\rangle = \frac{1}{\sqrt{2}}i(|0\rangle - i|1\rangle) \quad (38)$$

Then, the NV qubit evolves according to an operator $U_e(T_s/2, T_s) \simeq \bar{I}$ to reach a state

$$|\psi_3\rangle \simeq |\psi_2\rangle \quad (39)$$

By applying a $(\pi/2)_y$ -pulse, the NV qubit reaches the final state

$$|\psi_f\rangle = \frac{1}{2}i \begin{bmatrix} 1+i \\ 1-i \end{bmatrix} \quad (40)$$

which implies the NV qubit does not respond to B_x . Similarly, it does not respond to B_y .

In summary, the magnetic-field component aligned with the NV axis can be reconstructed without interference from the transverse components. A vector geomagnetic waveform can be reconstructed by utilizing NVEs with NV centers aligned with different crystallographic axes in a diamond lattice.

E. GENERATION OF NOISE WAVEFORM

Next, we will elaborate the relation between the Lorentzian spectrum of spin-bath noise and the associated time-varying magnetic field $b_z(t)$ in (9). The spin-bath noise is attributed to electron spin impurities in nitrogen (N) and nuclear spin impurities in ^{13}C , with the former dominating the decoherence in an NVE [30].

The spin-bath noise is modeled as classical stochastic magnetic field $b_z(t)$ following the Ornstein-Uhlenbeck (O-U) process, with the correlation function [35], [36]

$$C(t, t') = \gamma_e^2 \langle b_z(t)b_z(t') \rangle = b^2 e^{-|t-t'|/\tau_c} \quad (41)$$

where γ_e is the gyromagnetic ratio of the electron spin. The noise spectrum of magnetic field $b_z(t)$ is defined as [37]

$$S(\omega) = \gamma_e^2 \int_{-\infty}^{\infty} e^{i\omega t} \langle b_z(t')b_z(t) \rangle dt \text{ (rad}^2/\text{s}) \quad (42)$$

leading to the Lorentzian spectrum in (1) [35], and

$$b^2 = \frac{1}{2\pi} \int_{-\infty}^{\infty} S(\omega) d\omega \quad (43)$$

is the noise power of the spectrum [38]. The power spectral density (PSD) is defined as

$$P(\omega) = \frac{S(\omega)}{\gamma_e^2} \text{ (T}^2/\text{Hz}) \quad (44)$$

In this work, the O-U process is applied to generate noise magnetic field $b_z(t)$ [39], which is represented by a stationary Gaussian noise colored by the Lorentzian noise spectrum. The transition frequency (ω_0) is significantly higher than the cutoff frequency ($2\pi/\tau_c$) of the Lorentzian noise spectrum. Hence, the spin-bath noise induces pure dephasing on NV qubits in an NVE [38].

IV. SIMULATIONS AND DISCUSSIONS

A. SENSITIVITY ANALYSIS

Sensitivity has been widely used to evaluate the performance of a magnetometers. The sensitivity of short Ramsey sequence and spin-echo sequences used in this work will be analyzed in this subsection.

1) Short Ramsey Sequence

By exerting a short Ramsey sequence of sensing time T'_s to an NVE containing N NV centers, the ideal spin-projection-noise-limited sensitivity to the magnetic field is estimated as [22], [40]

$$\eta_R = \frac{1}{\gamma_e \sqrt{NT'_s}} \quad (45)$$

Due to the pure dephasing induced by the spin-bath noise on the NV qubits in an NVE, the sensitivity is reduced to [22]

$$\eta_R \simeq \frac{1}{\gamma_e \sqrt{NT'_s}} \frac{1}{e^{-(T'_s/T_2^*)^p}} \quad (46)$$

where $p = 1$ under Ramsey protocol and $p \simeq 1.5$ under spin-echo protocol for a ^{12}C sample [41].

In the simulations, four short Ramsey sequences ($N_R = 4$) of period $T'_s = 64\mu\text{s}$ each are applied over the sensing time of $T_s = 256\mu\text{s}$. With the parameters listed in Table 1, $T_2^* \simeq 70\mu\text{s}$ and $N = 10^8$, the sensitivity is estimated as $\eta_R \simeq 0.177 \text{ pT}/\sqrt{\text{Hz}}$, which is sufficient to accurately detect geomagnetic fluctuations of 0.1 nT under the spin-bath noise.

2) Spin-Echo Sequence

By exerting a spin-echo sequence on an NVE, the spin-projection-noise-limited sensitivity is estimated as [22], [40]

$$\eta_{se} \simeq \frac{\pi}{2} \frac{1}{\gamma_e \sqrt{N\tau_m}} \frac{1}{e^{-(\tau_m/T_2)^p}} \quad (47)$$

which is similar to that of the short Ramsey sequence, with the dephasing time T_2^* under Ramsey sequence replaced by T_2 . The factor $\pi/2$ is an uncertainty factor when applying an SE sequence for detecting a time-harmonic waveform [40].

With the Haar wavelets up to the eighth order, the shortest τ_m is $\tau_8 = 2\mu\text{s}$ and $T_2 \simeq 270\mu\text{s}$ as in Table 1. The poorest sensitivity is estimated as $\eta_{se} \simeq 0.631 \text{ pT}/\sqrt{\text{Hz}}$, corresponding to a minimum detectable field of $\delta B \simeq 0.109 \text{ nT}$ at 30 kHz, which is about the level of geomagnetic fluctuations in the VLF band. The sensitivity can be further improved by taking larger N or increasing the minimum τ_m .

B. ERROR ANALYSIS

Figs.3(a)-3(c) show the reconstructed geomagnetic waveform in the VLF band by using NVEs with different N 's. At $N = 10^8$, the geomagnetic fluctuation is well reconstructed and almost overlaps with the true waveform.

To evaluate the performance of our waveform reconstruction method, let's define a signal-to-noise ratio (SNR) between the signal and noise amplitudes as

$$SNR(\tilde{B}_{zp}) = \frac{\int_0^{T_{tot}} |\tilde{B}_f(t)| dt}{\int_0^{T_{tot}} |\tilde{B}_{zp}(t) - \tilde{B}_f(t)| dt} \quad (48)$$

where $\tilde{B}_f(t)$ and $\tilde{B}_{zp}(t)$ are the reconstructed geomagnetic waveform and an effective noise time series retrieved from the p th NV qubit in every NVE, respectively, and $T_{tot} = N_s T_s$ is the total sensing time on the waveform. In the simulations, we choose $N_s = 10$ and $T_s = 256\mu\text{s}$, with $T_s < T_2$ and $T_s < T_2^*$.

Fig.4 shows the SNR versus number of NV centers in an NVE. Some selected SNR values are also listed in Table 2. Note that the SNR under standard quantum limit (SQL) is proportional to \sqrt{N} at large N , under an ideal circumstance [22]. However, the simulated SNR increases with a trend of

$\sim N^{0.408}$ when $N \gtrsim 3 \times 10^7$, which may be attributed to the pure dephasing effect induced by the spin-bath noise. It was also claimed in [42] that the SNR versus the number of measurements was off the SQL, in the presence of decoherence.

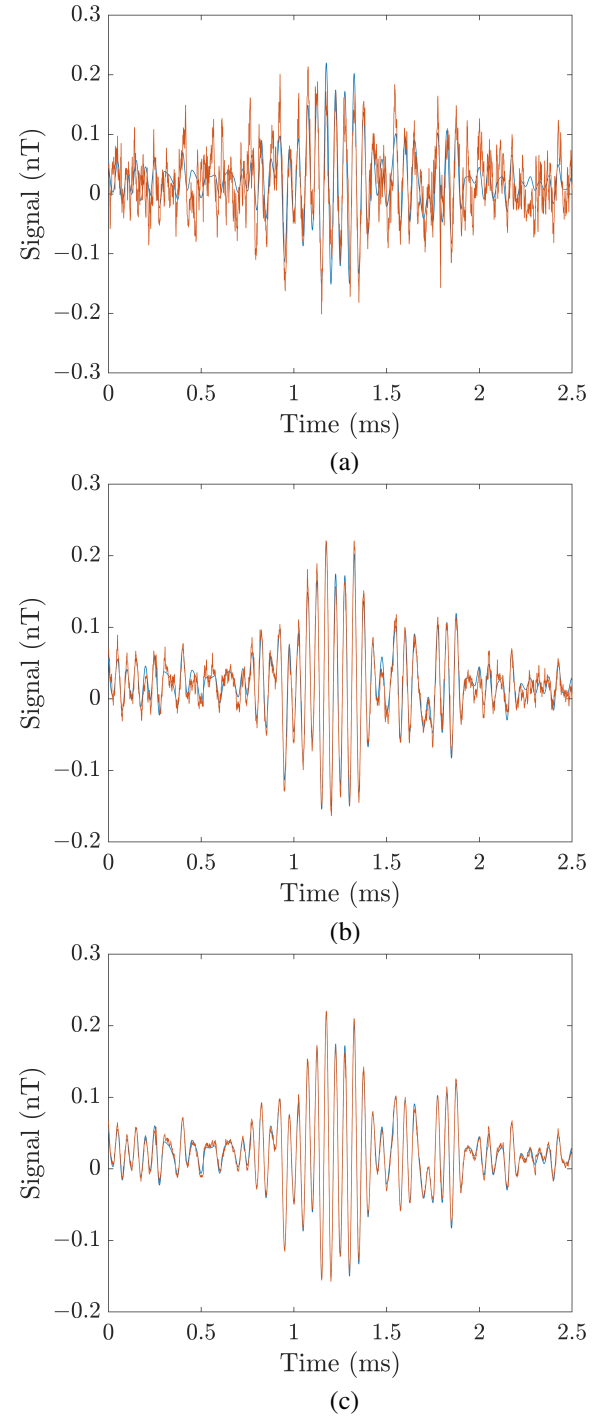


FIGURE 3. Reconstruction of geomagnetic fluctuations in VLF band by using NVEs with different N 's, —: true waveform, —: reconstructed waveform, (a) $N = 10^6$, (b) $N = 10^7$, (c) $N = 10^8$.

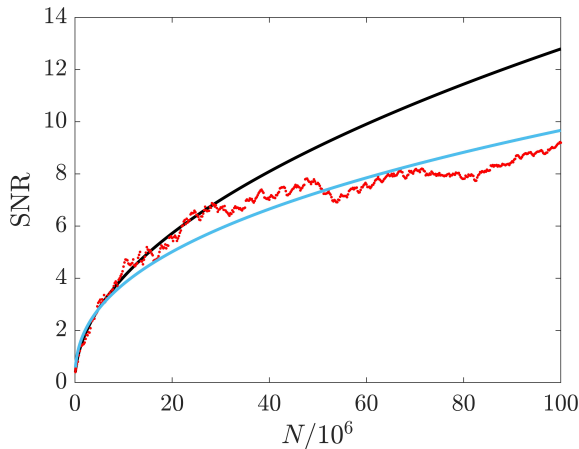


FIGURE 4. SNR versus N in an NVE, ———: standard quantum limit ($\text{SNR} \propto \sqrt{N}$), ·····: simulation results, ———: fit with simulation results ($\text{SNR} \propto N^{0.408}$).

TABLE 2. SNR versus N in an NVE.

N	SNR	N	SNR	N	SNR
2×10^5	0.512	2×10^6	1.535	2×10^7	5.544
5×10^5	0.749	5×10^6	3.111	5×10^7	7.653
10^6	1.211	10^7	4.446	10^8	9.196

C. NOISE SPECTROSCOPY AND PARAMETER EXTRACTION

In our simulation scenario, the magnitude of geomagnetic fluctuations is sub-nT, while that of noise can reach 100 nT. Thus, the fluorescence readout from a single NV qubit within an NVE will be dominated by the noise. To detect weak signal immersed in strong noise, NVEs with high density of NV centers are preferred. Ideally, N uncorrelated NV centers in an NVE can improve the sensitivity of signal detection by a factor of \sqrt{N} . In practice, factors like decoherence, dephasing and readout efficiency may deteriorate the sensitivity.

In order to reconstruct the noise spectrum, the fluorescence signal from individual NV qubits in an NVE can be readout with imaging technique if the NV density is sufficiently low. Although single NV readout was realizable from NVE with NV density of 10^{12} (cm $^{-3}$) [30], the NV density of 10^{14} (cm $^{-3}$) in this work might be too high to readout a single NV qubit. Thus, we propose a feasible noise spectroscopy method by collecting the fluorescence signal from batches of NV qubits in an NVE, contingent upon the spatial resolution of the available CCD chip.

The noise spectrum is reconstructed as follows:

- 1) Simulate $N = 10^8$ independent noise waveform, $\{b_{zp}(t)\}$, then superpose each to the geomagnetic fluctuations $B_f(t)$ to have $\{B_{zp}(t)\}$.
- 2) Assume there are N_b batches in one NVE, with $N' = N/N_b$ NV qubits in each batch, an effective field in the

q th batch is reconstructed as

$$\begin{aligned}\tilde{B}_{eq}(t) &= \frac{1}{N'} \sum_{p=1}^{N'} \tilde{B}_{zp}(t) \\ &= \frac{1}{N'} \sum_{p=1}^{N'} \left[d_p + \sum_{m=0}^M \sum_{n=0}^{2^m-1} c_{mn}^p h_m^n(t) \right] \quad (49)\end{aligned}$$

where $\tilde{B}_{zp}(t)$ is the reconstructed field from a single NV qubit, with $1 \leq p \leq N$. Note that the p th NV qubit in different NVEs senses different spin-bath noise, hence $\tilde{B}_{zp}(t)$ has no direct connection to any physical entity. Instead, $\tilde{B}_{zp}(t)$ can be viewed as an effective time series of noise that encodes the noise spectrum information embedded in the Haar coefficients and the dc offset coefficient.

- 3) The geomagnetic fluctuations is estimated by taking the average of $\{\tilde{B}_{eq}(t)\}$ from all the batches as

$$\tilde{B}_f(t) = \frac{1}{N_b} \sum_{q=1}^{N_b} \tilde{B}_{eq}(t) \quad (50)$$

- 4) An effective noise time series from the q th batch can be reconstructed by removing the geomagnetic fluctuations as

$$\tilde{b}_{eq}(t) = \tilde{B}_{eq}(t) - N' \tilde{B}_f(t) \quad (51)$$

- 5) Apply the Welch's method [43] on $\tilde{b}_{eq}(t)$ to reconstruct a noise spectrum from the q th batch as $\tilde{S}_q(\omega)$.
- 6) The final noise spectrum is obtained by taking the average over N_b batches as

$$\tilde{S}_{avg}(\omega) = \frac{1}{N_b} \sum_{q=1}^{N_b} \tilde{S}_q(\omega) \quad (52)$$

In the simulations, a batch is assumed to contain $N' = 100$ NV qubits.

Besides being limited by the spatial resolution of the CCD chip, the frequency resolution is limited by the per-interval sensing time T_s . To improve the frequency resolution by ten-fold, we concatenate 10 intervals of reconstructed waveform with length $T_s = 256\mu\text{s}$ to form a longer $\tilde{B}_{zp}(t)$ of length $T_{tot} = 2.56$ ms.

TABLE 3. Estimated parameters $\tilde{\Delta}$ and $\tilde{\tau}_c$ of noise spectrum by using PSO algorithm, with weighting factor ω^α in fitness function. True parameters are $\Delta = 30$ kHz and $\tau_c = 10\mu\text{s}$, $N' \times N_b = 10^6$.

N'	$\alpha = 1$		$\alpha = 0$	
	$\tilde{\Delta}$ (kHz)	$\tilde{\tau}_c$ (μs)	$\tilde{\Delta}$ (kHz)	$\tilde{\tau}_c$ (μs)
1	29.449	9.258	29.872	7.735
5	29.449	9.091	29.511	8.109
10	29.443	8.871	29.670	7.939
50	29.440	9.247	29.572	8.044
100	29.442	9.140	29.349	8.299

Next, the spin-bath coupling strength and the correlation time are estimated from $\tilde{S}_{avg}(\omega)$ as $\tilde{\Delta}$ and $\tilde{\tau}_c$, respectively,

by applying a particle swarm optimization (PSO) algorithm [44], [45] to solve the optimization problem

$$(\tilde{\Delta}, \tilde{\tau}_c) = \arg \min_{(\Delta, \tau_c)} \mathcal{J}(\Delta, \tau_c) \quad (53)$$

where

$$\mathcal{J}(\Delta, \tau_c) = \int |\tilde{S}_{avg}(\omega) - S(\omega, \Delta, \tau_c)|^2 \omega^\alpha d\omega \quad (54)$$

is the fitness function based on the difference between the simulated spectrum $\tilde{S}_{avg}(\omega)$ and the parameterized spectrum $S(\omega, \Delta, \tau_c)$.

Table 3 lists the estimated noise spectrum parameters $\tilde{\Delta}$ and $\tilde{\tau}_c$ by using the PSO algorithm, with $\alpha = 1$ and $\alpha = 0$, respectively. It is observed that under $N' \leq 100$, the change in N' has little effect on the estimation of noise spectrum parameters. Hence, the experimental constraints can be relaxed because the spatial resolution of a CCD chip is not required to resolve a single NV center.

The factor ω^α in the integrand of (54) adjusts the weighting on different frequency components. By setting $\alpha = 1$, more weighting is put near the cutoff frequency, yielding more accurate estimation of τ_c , as manifested in Table 3. By setting $\alpha = 0$, more weighting is put on the low-frequency components, leading to a more accurate estimation of Δ . If the true spectrum is a Lorentzian type, we propose to use $\alpha = 0$ to estimate Δ , and $\alpha = 1$ to estimate τ_c .

Fig.5 shows the true Lorentzian spectrum of a ^{12}C NVE sample and the reconstructed spectrum with $N' = 100$. The noise spectrum is reconstructed accurately as compared to the true noise spectrum, down to the low-frequency components ($f \lesssim 10$ kHz). The frequency spacing in the simulated spectrum is $\Delta f \propto 1/T_{tot}$. The simulated spectrum deviates from the true spectrum at $f \gtrsim 100$ kHz, which is attributed to the truncated order ($M = 8$) of the inverse Haar wavelet transform we adopted.

The simulated spectrum manifests a small dip around $f \sim 5$ kHz, leading to little error in the estimated spectrum parameters. We suspect this dip may come from the residual signal of geomagnetic fluctuations which happen to be in the VLF band (3 to 30 kHz). Hence, another noise spectrum is reconstructed from the simulated noise with $B_f = 0$, namely, $B_z(t) = b_z(t)$ in (9). The results are marked by cyan circles in Fig.5(b), which overlap with their counterparts with $B_f \neq 0$ (red dots). Thus, the dip in the simulated spectrum is not attributed to the residual geomagnetic fluctuations.

It is observed that using only the Haar wavelet method (without short Ramsey sequences), the reconstructed noise spectrum significantly deviates from the true spectrum at $f < 3$ kHz. In the simulations, 10 effective noise time series are concatenated to improve the frequency resolution by tenfold. We conjecture the dip in the reconstructed noise spectrum may be attributed to the discontinuities at junctions between two effective noise time series. The sensing time of each effective noise time series is 256 μs , which is transformed to a frequency of 3.906 kHz, about where the noise spectrum dip appears.

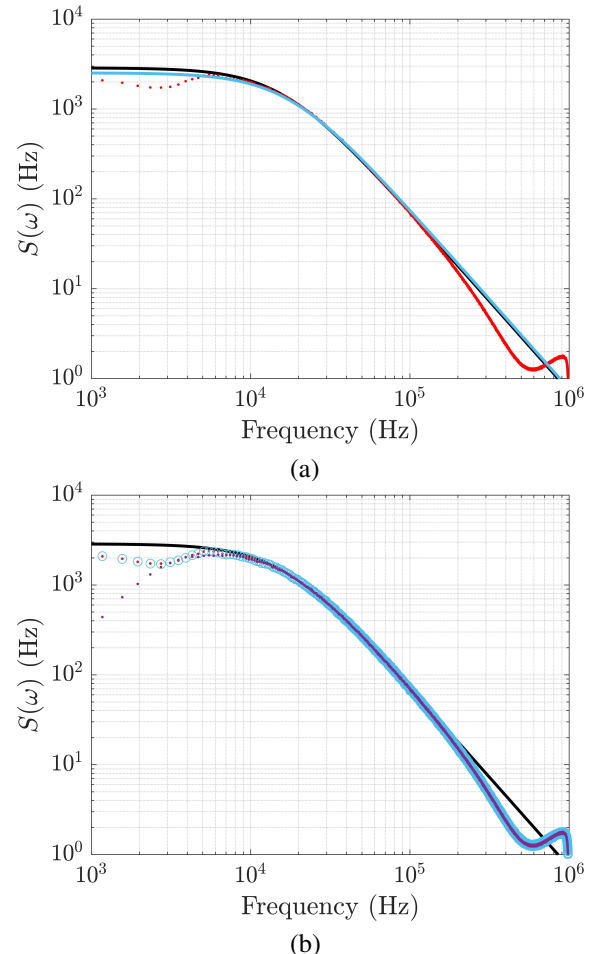


FIGURE 5. Lorentzian noise spectrum of ^{12}C NVE sample. (a) —: true spectrum $S(\omega)$, ···: simulated $\tilde{S}_{avg}(\omega)$ with $N' = 100$, —: spectrum obtained by fitting $\tilde{S}_{avg}(\omega)$ to Lorentzian spectrum $S(\omega, \Delta, \tau_c)$ with PSO algorithm, $\alpha = 1$, (b) Comparison with $\tilde{S}_{avg}(\omega)$ reconstructed under different settings, $N' = 100$, —: true spectrum $S(\omega)$, ···: proposed method and default settings, ○○○: proposed method but without geomagnetic fluctuations ($B_f = 0$), ···: Haar wavelet method only, without short Ramsey sequences.

In summary, the proposed hybrid method can significantly improve the fidelity of reconstructed noise spectrum at low frequencies, except with a small dip around a few kHz.

D. COMPARISON WITH EXISTING WAVEFORM RECONSTRUCTION AND NOISE SPECTROSCOPY METHODS

Our proposed method combines the advantages of the direct Ramsey sensing method and the Haar wavelet method. The direct Ramsey sensing method is the most straightforward waveform reconstruction method [46], which interrogates a brief interval of the signal at a time. The signal can be directly recovered without post-processing due to the small accumulated phase. However, the direct Ramsey sensing method has limited time resolution and its sensitivity is poor due to its brief sensing time. On the other hand, the Haar wavelet method in [27] cannot accurately estimate low-frequency components in the noise spectrum.

These two problems can be resolved with the proposed hybrid short Ramsey-Haar wavelet method. The purpose of imposing consecutive brief sensing periods in direct Ramsey sensing method is to preserve high-frequency components in a waveform, which can be achieved with the Haar wavelet method. On the other hand, the short Ramsey sequences (with much longer sensing time than that in the direct Ramsey sensing method) are used to restore the low-frequency components.

In [46], an arbitrary waveform was restored with quantum sensors without reconstruction process. Although a fine time resolution of 20 ns is achieved, its sensitivity is only about $4 \mu\text{T}/\sqrt{\text{Hz}}$, and the target signal has to be repeated at least twice. Thus, it is not suitable for the sensing of very weak and arbitrary geomagnetic fluctuations.

In contrast, our proposed method is capable of reconstructing an arbitrary waveform in the kHz range at 0.01 nT level, achieving the sensitivity of $0.63 \text{ pT}/\sqrt{\text{Hz}}$. The Haar wavelets are implemented with SE sequences, prolonging qubit dephasing time [27]. The shortcoming of inaccurate estimation on low-frequency components in the noise spectrum can be effectively mitigated with the proposed short Ramsey sequences.

In [27], it was claimed that a waveform with 2^n points can be reconstructed with only $O(n)$ runs. However, the waveform information cannot be collected by the qubits during the intervals when laser pulses are applied to initialize and readout the state, which may lead to inaccurate reconstruction of a weak arbitrary waveform.

Conversely, the proposed hybrid short Ramsey-Haar wavelet method is implemented with multiple NVEs. Each NVE can be controlled independently to ensure that the entire geomagnetic waveform is covered. Moreover, the proposed method can be used to conduct noise spectroscopy.

Our proposed method is implemented with $N_e = O(2^n)$ NVEs, with each NVE responsible for a designate dc offset coefficient or Haar coefficient. It takes only one run to determine all the N_e coefficients for inverse Haar wavelet transform, making the proposed method ready for parallel processing and real-time operation.

Dynamical decoupling (DD)-based methods have been proposed for noise spectroscopy [25], [26], [47]. By increasing the number of pulses in a DD sequence, the filter function in the frequency domain gains a higher frequency selectivity, and the qubit decoherence and dephasing can also be mitigated to extend the total sensing time.

However, DD-based noise spectroscopy suffers from poor accuracy and sensitivity at low-frequency components [47], because it is difficult to realize a DD sequence with very long inter-pulse interval. This problem can be overcome with our proposed method or the Walsh-based method. Our proposed method shares many attributes with the Walsh-based method, which was also proposed for waveform reconstruction [48] and noise spectroscopy [49].

The Walsh-based method exploits different DD protocols to implement Walsh functions of different orders. Walsh

functions form a complete orthonormal basis, as Haar functions do, to represent an arbitrary waveform. The Walsh-based method requires the first 2^n Walsh coefficients to reconstruct a 2^n -point time series. Similarly, our proposed method requires the $N_e = O(2^n)$ coefficients to reconstruct a 2^n -point waveform.

While the Walsh basis is implemented with Ramsey, spin-echo, periodic dynamical decoupling (PDD) and Carr-Purcell-Meboom-Gill (CPMG) sequences, the proposed method requires only short Ramsey and spin-echo sequences, which is more concise than the former in terms of MW control.

In addition, the zeroth-order function in the Walsh basis in [48] is directly implemented with the conventional Ramsey sequence, which might lead to inaccurate estimation of waveform or noise spectrum if the time-domain signal (or noise) deviates from zero during the sensing period or has a large non-zero mean. This defect can be effectively mitigated by adopting the proposed short Ramsey sequences with a properly chosen N_R .

V. CONCLUSIONS

A combined use of short Ramsey sequences and Haar wavelet method is proposed for the first time to simultaneously reconstruct very weak magnetic fluctuations and spin-bath noise spectrum using NV ensembles. The geomagnetic fluctuations in the kHz range at 0.01 nT level can be reconstructed with the sensitivity of $0.63 \text{ pT}/\sqrt{\text{Hz}}$. A set of NVEs are used to estimate dc offset coefficients and Haar coefficients by exerting designate short Ramsey or spin-echo sequence for MW control on each NVE. The short Ramsey sequences enable faithful restoration of low-frequency components in the noise spectrum, while the Haar wavelet method can accurately reconstruct high-frequency components.

Simulations with each NVE containing $N = 10^8$ NV qubits validate accurate reconstruction of geomagnetic fluctuations and spin-bath noise spectrum. The effect of NV-center population in an NVE on the reconstruction of geomagnetic fluctuations is studied, and the effect of batch size on the reconstruction of noise spectrum is also analyzed. In the presence of pure dephasing induced by the spin-bath noise, the sensitivity and SNR drop from the standard quantum limit of \sqrt{N} to $N^{0.4}$ at large N . A particle swarm optimization algorithm is used to accurately estimate the spin-bath coupling strength and correlation time of the spin-bath noise spectrum. In the future, quantum sensors based on the proposed method can be mounted on board of nano-satellites, forming a global quantum sensing network.

ACKNOWLEDGMENT

The authors would like to acknowledge the DEMETER Scientific Mission Center and CDPP (Centre des Données de la Physique des Plasmas) for providing the magnetic field observation data in <https://cdpp-archive.cnes.fr/>.

REFERENCES

- [1] C. L. Degen, F. Reinhard, and P. Cappellaro, "Quantum sensing," *Rev. Mod. Phys.*, vol. 89, 035002, Jul. 2017.
- [2] D. J. McCloskey et al., "Enhanced Widefield Quantum Sensing with Nitrogen-Vacancy Ensembles Using Diamond Nanopillar Arrays," *ACS Appl. Mater. Interfaces*, vol. 12, no. 11, pp. 13421-13427, Feb. 2020.
- [3] C. Foy et al., "Wide-Field Magnetic Field and Temperature Imaging Using Nanoscale Quantum Sensors," *ACS Appl. Mater. Interfaces*, vol. 12, no. 23, pp. 26525-26533, Apr. 2020.
- [4] X. Wang et al., "Quantum diamond magnetometry for navigation in GNSS denied environments," *arXiv:2302.06187 [math.OC]*, Feb. 2023.
- [5] N. Aslam et al., "Quantum sensors for biomedical applications," *Nat. Rev. Phys.*, vol. 5, pp. 157-169, Feb. 2023.
- [6] F. Casola, T. van der Sar, and A. Yacoby, Probing Condensed Matter Physics with Magnetometry Based on Nitrogen-Vacancy Centres in Diamond, *Nat. Rev. Materials*, vol. 3, 17088, Jan. 2018.
- [7] Q. Wang et al., "Hybrid NV Center Magnetometer with Directional Vector Resolution Based on Magnetic Flux Concentrators," *IEEE Sensors J.*, vol. 23, no. 12, pp. 12719-12726, Jun. 2023.
- [8] N. Olsen and C. Stolle, "Satellite Geomagnetism," *Ann. Rev. Earth Planetary Sci.*, vol. 40, pp. 441-465, May 2012.
- [9] J. H. Kim and H.-Y. Chang, "Geomagnetic Field Variations Observed by INTERMAGNET during 4 Total Solar Eclipses," *J. Atmos. Solar-Terr. Phys.*, vol. 172, pp. 107-116, Jul. 2018.
- [10] C. Constable, "Earth's electromagnetic environment," *Surveys Geophys.*, vol. 37, pp. 27-45, Dec. 2015.
- [11] Z. Zhima et al., "Possible Ionospheric Electromagnetic Perturbations Induced by the Ms7.1 Yushu Earthquake," *Earth, Moon, and Planets*, vol. 108, pp. 231-241, May 2012.
- [12] M. Parrot et al., "The Magnetic Field Experiment IMSC and Its Data Processing Onboard DEMETER: Scientific Objectives, Description and First Results," *Planetary Space Sci.*, vol. 54, pp. 441-455, Apr. 2006.
- [13] CDPP Archive. [Online]. Available: <http://cdpp-archive.cnes.fr/>. Accessed on: Jul. 13, 2023.
- [14] Y.-Y. Ho, H.-K. Jhuang, Y. Z. Su, and J. B. Liu, "Seismo-ionospheric anomalies in total electron content of the GIM and electron density of DEMETER before the 27 February 2010 M8.8 Chile earthquake," *Advances in Space Res.*, vol. 51, pp. 2309-2315, Jun. 2013.
- [15] K. Ryu et al., "Suspected Seismo-Ionospheric Coupling Observed by Satellite Measurements and GPS TEC Related to the M 7.9 Wenchuan Earthquake of 12 May 2008," *J. Geophys. Res.: Space Phys.*, vol. 119, no. 12, pp. 10305-10323, Dec. 2014.
- [16] M. Parrot, A. L. Buzzi, O. Santolik, J.-J. Berthelier, J. A. Sauvaud, and J.-P. Lebreton, "New observations of electromagnetic harmonic ELF emissions in the ionosphere by the DEMETER satellite during large magnetic storms," *J. Geophys. Res.: Space Phys.*, vol. 111, A08301, Jan. 2006.
- [17] Z. Zhima et al., "Storm Time Evolution of ELF/VLF Waves Observed by DEMETER Satellite, Journal of Geophysical Research: Space Physics," *J. Geophys. Res.: Space Phys.*, vol. 119, pp. 2612-2622, Apr. 2014.
- [18] J. M. G. Merayo et al. "The Swarm Magnetometry Package," in *Small Satellites for Earth Observation: Selected Contributions*. Springer, 2008.
- [19] W. Kozlowski and S. Wehner, "Towards Large-Scale Quantum Networks," in *NANOCOM '19: Proceedings of the Sixth Annual ACM International Conference on Nanoscale Computing and Communication*, Sep. 2019, p. 3.
- [20] E. Pelucchi et al., "The Potential and Global Outlook of Integrated Photonics for Quantum Technologies," *Nat. Rev. Phys.*, vol. 4, pp. 194-208, Mar. 2022.
- [21] T. Wolf et al., "Subpicotesla Diamond Magnetometry," *Phys. Rev. X*, vol. 5, 041001, Oct. 2015.
- [22] J. F. Barry et al., "Sensitivity Optimization for NV-Diamond Magnetometry," *Rev. Mod. Phys.*, vol. 92, 015004, Mar. 2020.
- [23] K.-M. C. Fu, G. Z. Iwata, A. Wickenbrock, and D. Budker, "Sensitive Magnetometry in Challenging Environments," *AVS Quantum Science*, vol. 2, 044702, Dec. 2020.
- [24] A. M. Souza, G. A. Álvarez, and D. Suter, "Robust Dynamical Decoupling for Quantum Computing and Quantum Memory," *Phys. Rev. Lett.* vol. 106, 240501, Jun. 2011.
- [25] J. Bylander et al., "Noise Spectroscopy through Dynamical Decoupling with a Superconducting Flux Qubit," *Nat. Phys.*, vol. 7, pp. 565-570, May 2011.
- [26] P. Szałkowski, G. Ramon, J. Krzywda, D. P. Kwiatkowski, and Ł. Cywiński, "Environmental Noise Spectroscopy with Qubits Subjected to Dynamical Decoupling," *J. Phys.: Condensed Matter*, vol. 29, 333001, Jul. 2017.
- [27] N. Xu et al., "Wavelet-Based Fast Time-Resolved Magnetic Sensing with Electronic Spins in Diamond," *Phys. Rev. B*, vol. 93, 161117, Apr. 2016.
- [28] Y. Hatano et al., "Simultaneous thermometry and magnetometry using a fiber-coupled quantum diamond sensor," *Appl. Phys. Lett.* vol. 118, 034001, Jan. 2021.
- [29] L. Pham et al., "Magnetic field imaging with nitrogen-vacancy ensembles," *New J. Phys.* vol. 13, 045021, Apr. 2011.
- [30] N. Bar-Gill et al., "Suppression of Spin-Bath Dynamics for Improved Coherence of Multi-Spin-Qubit Systems, *Nature Communications*," *Nat. Commun.*, vol. 3, 858, Jan. 2012.
- [31] S. Lin et al., "Temperature-Dependent Coherence Properties of NV Ensemble in Diamond up to 600 K," *Phys. Rev. B*, vol. 104, 155430, Oct. 2021.
- [32] A. Nits et al., "gwastro/pycbc: v2.2.1 release of PyCBC," doi: 10.5281/zenodo.8190155, Jul. 2023.
- [33] S. Mallat, *A Wavelet Tour of Signal Processing: The Sparse Way*, 3rd Ed. Academic Press, 2009.
- [34] G. Strang, "Wavelet Transforms versus Fourier Transforms," *Bulletin of the American Mathematical Society*, vol. 28, pp. 288-306, Apr. 1993.
- [35] Z.-H. Wang and S. Takahashi, "Spin decoherence and electron spin bath noise of a nitrogen-vacancy center in diamond," *Phys. Rev. B*, vol. 87, 115122, Mar. 2013.
- [36] Y. Chou, S.-Y. Huang, and H.-S. Goan, "Optimal control of fast and high-fidelity quantum gates with electron and nuclear spins of a nitrogen-vacancy center in diamond," *Phys. Rev. A*, vol. 91, 052315, May 2015.
- [37] M. Joos, D. Bluvstein, Y. Lyu, D. Weld, and A. Jayich, "Protecting qubit coherence by spectrally engineered driving of the spin environment," *npj Quantum Inf.*, vol. 8, 47, Apr. 2022.
- [38] W. Yang, W.-L. Ma, and R.-B. Liu, "Quantum Many-Body Theory for Electron Spin Decoherence in Nanoscale Nuclear Spin Baths," *Rep. Prog. Phys.*, vol. 80, 016001, Nov. 2016.
- [39] E. Bibbona, G. Panfilo, and P. Tavella, "The Ornstein-Uhlenbeck Process as a Model of a Low Pass Filtered White Noise," *Metrologia*, vol. 45, pp. S117-S126, Dec. 2008.
- [40] J. M. Taylor et al., "High-Sensitivity Diamond Magnetometer with Nanoscale Resolution, *Nature Physics*," *Nat. Phys.*, vol. 4, pp. 810-816, Sep. 2008.
- [41] E. Bauch et al., "Decoherence of ensembles of nitrogen-vacancy centers in diamond," *Phys. Rev. B*, vol. 102, 134210, Oct. 2020.
- [42] A. Bienfait et al., "Reaching the Quantum Limit of Sensitivity in Electron Spin Resonance," *Nat. Nanotechnology*, vol. 11, pp. 253-257, Dec. 2015.
- [43] P. Welch, "The Use of Fast Fourier Transform for the Estimation of Power Spectra: A Method Based on Time Averaging over Short, Modified Periodograms," *IEEE Trans. Audio Electroacoustics*, vol. 15, no. 2, pp. 70-73, Jun. 1967.
- [44] M. Clerc and J. Kennedy, The particle swarm-explosion, stability, and convergence in a multidimensional complex space, *IEEE Trans. Evol. Comput.*, vol. 6, no. 1, pp. 58-73, Feb. 2002
- [45] G. Venter and J. Sobieszczański-Sobieski, "Particle swarm optimization," *AIAA Journal*, vol. 41, no. 8, pp. 1583-1589, Aug. 2003.
- [46] J. Zopes and C. L. Degen, "Reconstruction-free quantum sensing of arbitrary waveforms," *Phys. Rev. Appl.*, vol. 12, 054028, Nov. 2019.
- [47] M. J. Biercuk, A. C. Doherty, and H. Uys, "Dynamical decoupling sequence construction as a filter-design problem," *J. Phys. B: Atomic, Molecular and Optical Physics*, vol. 44, 154002, Jul. 2011.
- [48] A. Cooper, E. Magesan, H. N. Yum, and P. Cappellaro, Time-Resolved Magnetic Sensing with Electronic Spins in Diamond, *Nat. Commun.*, vol. 5, 3141, Jan. 2014.
- [49] G. Wang et al., "Digital noise spectroscopy with a quantum sensor," *arXiv:2212.09216 [quant-ph]*, Dec. 2022.



CHOU-WEI KIANG received his B.S. degree in electrical engineering from National Taiwan University, Taipei, Taiwan, in 2022. He is currently a research assistant in the Quantum Electronics Laboratory, National Taiwan University. From 2020 to 2023, he was a research assistant in the Group of Electromagnetic Applications, National Taiwan University, where he worked on quantum sensing and remote sensing. His research interests include quantum science and engineering, quantum information processing, optics and electromagnetics, remote sensing, radar and sonar imaging, and signal processing applications.



JEAN-FU KIANG (Life Senior, IEEE) received his Ph.D. degree in electrical engineering from the Massachusetts Institute of Technology, Cambridge, MA, USA, in 1989.

Since 1999, he has been a Professor with the Department of Electrical Engineering and Graduate Institute of Communication Engineering, National Taiwan University. His research interest is to explore different ideas, theories and methods on various electromagnetic phenomena and possible applications, including remote sensing, radar signal processing, antennas, phased arrays, propagation, scattering, communications, and so on. Some of his works can be viewed in his website: http://cc.ee.ntu.edu.tw/~jfkiang/selected_publications.html

• • •